Sea-surface temperature induced variability of the Southern Annular Mode in an atmospheric general circulation model

Tianjun Zhou and Rucong Yu

State Key Laboratory of Numerical Modeling for Atmospheric Sciences and Geophysical Fluid Dynamics, Institute of Atmospheric Physics, Chinese Academy of Sciences, Beijing, China

Received 13 September 2004; revised 6 October 2004; accepted 19 November 2004; published 22 December 2004.

[1] The reproducibility of the Southern Hemisphere Annular Mode (SAM) is examined by using the NCAR CAM2 model forced with historical sea surface temperature covering the time period of 1950–2000. There is some correspondence (low however significant correlation) between the simulation and observation in the temporal evolution of the SAM, indicating if global SSTs are known and prescribed to the model, there would be some predictability to the SAM. The reproducibility is greater during austral summer than winter, and the source of much of the reproducibility is tropical Pacific SST, with equatorial Pacific warm event corresponds to a negative phase SAM in austral summer. There is a hint that this result is model independent. Working with ensembles improves the reproducibility. *INDEX TERMS:* 1620 Global Change: Climate dynamics (3309); 1610 Global Change: Atmosphere (0315, 0325); 3319 Meteorology and Atmospheric Dynamics: General circulation; 3339 Meteorology and Atmospheric Dynamics: Ocean/atmosphere interactions (0312, 4504); 3334 Meteorology and Atmospheric Dynamics: Middle atmosphere dynamics (0341, 0342). **Citation:** Zhou, T., and R. Yu (2004), Sea-surface temperature induced variability of the Southern Annular Mode in an atmospheric general circulation model, *Geophys. Res. Lett.*, *31*, L24206, doi:10.1029/2004GL021473.

1. Introduction

[2] The Southern Hemisphere Annular Mode (SAM) or the Antarctic Oscillation (AAO) is one of the main variability patterns of the atmospheric circulation in the Southern Hemisphere (SH) throughout the year. It refers to a large scale alternation of atmospheric mass between mid-latitude and high-latitude [*Kidson*, 1988, 1999; *Gong and Wang*, 1999; *Thompson and Wallace*, 2000]. The SAM has a roughly zonally symmetric structure and emerges as the leading empirical orthogonal function (EOF) mode of the SH sea level pressure (SLP) with associated patterns of temperature, zonal wind, and geo-potential height from the surface to the stratosphere [*Thompson and Wallace*, 2000]. The SAM is known to be strongly linked to climate anomalies over the middle and high latitude SH [*Mo*, 2000; *Watterson*, 2000; *Thompson et al.*, 2000; *Clare et al.*, 2002; *Hall and Visbeck*, 2002; *Silvestri and Vera*, 2003]. The SAM signals can even be found out of the SH, one example is its potential impact on the East Asian summer monsoon [*Xue et al.*, 2003; *Nan and Li*, 2003].

0094-8276/04/2004GL021473$05.00

[3] *Thompson and Wallace* [2000] argue that the SAM and the Arctic Oscillation (AO) are dynamically similar, that there have been recent trends in these patterns. The forcing of these trends has received considerable attention. While the issue for the AO is complex and there is no consensus on the stratospheric involvement in the evolution of the AO [*Shindell et al.*, 1999; *Fyfe et al.*, 1999; *Kushner et al.*, 2001], by contrast, the SAM trend is found to be consistent with the stratospheric ozone loss [*Sexton*, 2001; *Thompson and Solomon*, 2002], and the response of the SAM to increasing CO_2 displays an upward trend in transient greenhouse warming integrations [*Shindell et al.*, 1999; *Fyfe et al.*, 1999; *Kushner et al.*, 2001; *Stone and Weaver*, 2001].

[4] Although the mechanism of the SAM limits its own reproducibility [*Limpasuvan and Hartmann*, 2000; *Watterson*, 2001], any potential useful predictions of the SAM evolution would greatly benefit the regional social and economic development. Prediction of short-term atmospheric climate anomalies depends largely on the impact of sea surface temperature (SST). *Kidson and Watterson* [1999] noted that the SAM was unpredictable on the submonthly timescale. Here we examine the SST-induced reproducibility of the SAM at monthly and interannual scales based on a set of atmospheric climate model ensembles forced by observed historical SST data. The model datasets come from the National Center for Atmospheric Research (NCAR) CAM 2.0.1 global SST 15-member ensemble. Fifteen simulation runs were carried out using CAM 2.0.1 and observed SST's from January 1950 to December 2000 by NCAR climate variability working group. The model is a global primitive equation spectral model with T42 triangular truncation and 26 vertical levels. Details of the model are described at the NCAR website (available at http://www.ccsm.ucar.edu/models/ccsm2.0.1/cam/camUsersGuide/). The observational data of sea level pressure (SLP) is taken from the National Centers for Environmental Prediction (NCEP)/NCAR reanalysis data [*Kalnay et al.*, 1996], and the time covers the same period of model simulation. Both the model and the observational data employ a regular grid of 2.5° by 2.5°.

2. Results

2.1. Monthly Scale

[5] The intensity of the SAM (hereinafter SAMI) is defined using the normalized leading PC of EOF analysis. A positive sign of PC corresponds to a positive polarity of the SAM. The substantial trend in the observational SAMI is attributed to trends in stratospheric ozone depletion and greenhouse gas concentration, since the model simulations

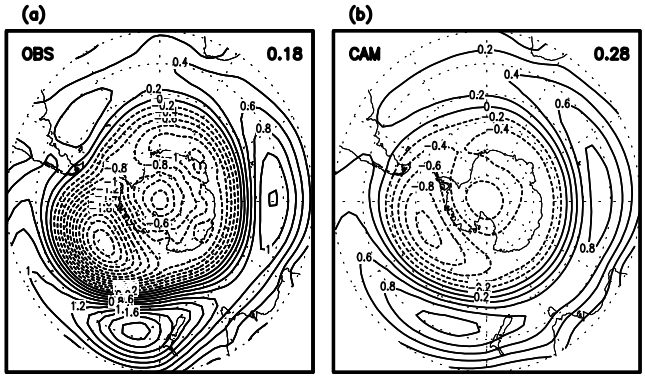

Figure 1. (a) Observed and (b) ensemble-mean EOF1 for monthly SLP anomalies (scaled by the standard deviation of their associated principal component time series). The fraction of explained variance is indicated in the right upper corner of the map.

contain neither of these features, comparison of the model SAMI should be made with the detrended observational SAMI. In the following analyses, detrending is done on the observational SLP data before the EOF analysis. Another benefit of detrending is that this can greatly reduce the data discontinuity caused by the observation system changes in late 1970s [*Marshall*, 2003]. The seasonal cycle is removed prior to the analyses. Gridded data are weighted by the cosine of latitude.

[6] An ensemble-mean of 15 simulations with different initial conditions is firstly analyzed. The model analysis parallels the observational analysis to facilitate comparison. Figure 1 displays the first leading EOF pattern for the SH (south of 20°S) monthly SLP. The time period covers 1950–2000, i.e., there are a total of 612 months. The leading modes are identified as SAM in both the observation and the simulation. The model presents a quite realistic SAM mode, having a pattern correlation of 0.94 with the observation. The model SAM explains 28.1% of the variability, apparently higher than that of the observation, which is 18.0% (the percentage increases to 23.8% without detrending).

[7] The observed and the simulated SAMI are given in Figure 2. The original observational SAMI has an obvious linear trend in the past decades (Figure 2a). Notice this trend is removed in the following analysis. The detrended observational SAMI (Figure 2b) has a correlation coefficient of 0.20 with the simulation (Figure 2c). There is some persistence in the sign of the SAM over the season. The first-order autocorrelation coefficient of the SAMI is 0.37 in the observation and 0.72 in the simulation, implying samples not random and the number of truly independent samples should be fewer than 612. According to *Dawdy and Matalas* [1964], the effective sample size is proved to be 355, which is far less than the original sample size. Note that the 99% confidence level without the adjustment of sample size is approximately 0.104, while the 99% confidence level with the adjustment is 0.136. The correlation coefficient of 0.20 between the detrended observation and the simulation indicated above is therefore significant at 99% confidence level, indicating a modest potential reproducibility.

[8] Following *Stone and Weaver* [2001], the model SAMI can also be calculated by projecting the simulated monthly SLP anomalies onto the observational SAM pattern shown in Figure 1a. This new index has a simultaneous correlation coefficient of 0.21 with the observation and 0.99 with the previous model SAMI shown in Figure 2c. The monthly-scale persistence keeps unchanged. Considering the close resemblance of the model SAM spatial pattern with the observation, this consistency is understandable.

[9] To explore the spread or convergence among ensemble members, SAMI for every individual ensemble member is calculated by projecting SLP anomalies upon the ensemble-mean SAM pattern shown in Figure 1b. Correlation coefficients in between the observed SAMI, the ensemble-mean SAMI, and every individual ensemble member's SAMI are listed in Table 1. Correlation coefficients between the observation and each individual simulation vary from −0.01 to 0.15. The ensemble-mean SAMI has the highest correlation with the observation and working with ensembles clearly improves the reproducibility. All single member's SAMI have significant correlations with the ensemble-mean SAMI, correlation coefficients ranging from 0.32 to 0.46, also indicating a potential reproducibility.

[10] Each ensemble member's SAMI can also be defined by using its own PC of EOF analysis, and this allows individual member's SAM to manifest as a mode that may be different from that in the ensemble-mean. The results are comparable with those listed in Table 1, implying a negligible impact of the SAMI definition. Each ensemble member's SAM mode seems to be close to that of the ensemble-mean, and the pattern shifts of SAM among ensemble members are substantially small. The internal dynamics of the atmosphere thus mainly disturbs the time evolution of the SAM rather than its spatial pattern. This is further confirmed by the pattern correlations between the ensemble-mean leading EOF and individual member's leading EOF, ranging from 0.93 to 0.97.

[11] To quantitatively reveal the model's external and internal SAMI variability, defined respectively as the model's response to prescribed SST variations and the model's random variation, the analysis of variance technique is employed as in *Li* [1999]. Analysis on the monthly SAMI

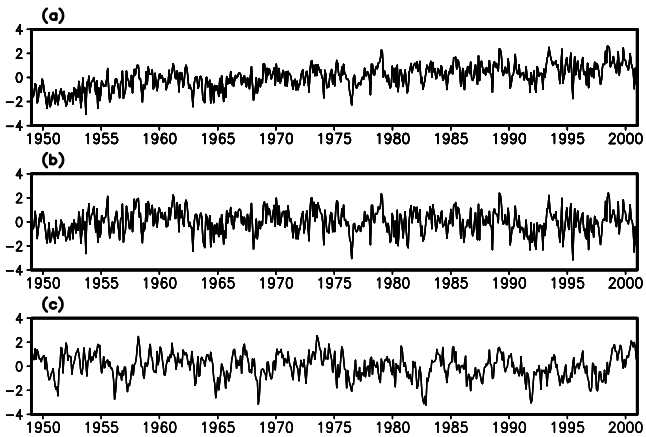

Figure 2. The monthly SAM index for (a) the observation without detrending, (b) the observation after detrending, and (c) the ensemble-mean.

Table 1. Correlation Coefficients in Between Observed SAMI, Ensemble-Mean SAM, and Single-Member SAMI[a]

	Obs	Ens	s1	s2	s3	s4	s5	s6	s7	s8	s9	s10	s11	s12	s13	s14	s15
Obs	**1.0**	**0.20**	0.09	0.06	0.05	0.10	0.08	0.05	−0.01	0.07	0.08	0.07	0.09	0.15	0.08	0.14	0.07
Ens	**0.20**	**1.0**	**0.42**	**0.37**	**0.33**	**0.44**	**0.40**	**0.45**	**0.35**	**0.46**	**0.31**	**0.39**	**0.42**	**0.43**	**0.37**	**0.40**	**0.32**

[a]Here "s1" indicates single member 1 and similar for others. Single member's SAMI is calculated by projecting the SLP anomalies onto the ensemble-mean SAM pattern. Bold numbers have 95% confidence level.

shows that the internal atmospheric dynamics accounts for 86.8% and the external forcing accounts for 13.2% of the total variance. The internal noise is much larger than the forced signal, and this is partly the reason why the CAM model only has a modest reproducibility in simulating monthly SAM oscillation.

2.2. Interannual Scale and Its Seasonal Dependence

[12] Although SAM changes little throughout the year, it is still valuable to test the seasonal dependence of the CAM model in reproducing the interannual SAM variability. For comparison with *Carril and Navarra* [2001], EOF analysis is performed on the austral summer (January–February–March, JFM) and winter (July–August–September, JAS) separately. The SAM mode stands out as the first EOF mode both in the observation and in the simulation, and it explains more variance in austral summer than in winter (24% versus 21% in observation and 57% versus 34% in simulation, figure omitted). The model reproduces a better austral summer SAM mode. The simulated SAM has a pattern correlation coefficient of 0.83 in JFM and 0.71 in JAS with the observation. The observed and the simulated SAMI are also expressed in terms of the normalized PCs of EOF analyses (Figure 3). Both of them have a nearly zero first-order autocorrelation coefficients. The time oscillation of CAM SAM in the austral summer presents good agreement with the detrended observational index, and the correlation coefficient between them is 0.31, which has 95% confidence level. Both the spatial and the temporal oscillation of the CAM SAM are therefore realistic in the austral summer. For the austral winter, however, the CAM model fails to reproduce the observed temporal SAM oscillation, and no significant correlation is found between the simulated and the observed SAMIs. Whilst the model can successfully reproduce the spatial pattern of the SAM in both seasons, its capability in representing the temporal oscillation is seasonally dependent, and the austral summer SAM has a higher reproducibility. Considering similar results were found by using ECHAM model and ECMWF reanalysis data for the period 1979–1993 [*Carril and Navarra*, 2001], there is a hint that this result is model-independent and data-independent.

[13] The seasonal SAMI can be constructed in another way. The monthly SAM index values shown in Figure 2b and 2c are averaged into JFM and JAS seasonal means (figures omitted). For observation, the new SAMI has a correlation coefficient of 0.94 in JAS and 0.98 in JFM respectively with the seasonal EOF mode-based SAMI shown in Figure 3 (solid lines). For simulation, the corresponding correlation coefficient is 0.96 in JAS and 0.99 in JFM. The seasonal and monthly data based basis functions thus have negligible differences in the constructed SAM indices due to the weak seasonality of the SAM pattern [*Thompson and Wallace*, 2000]. The correlation coefficient between the simulated and the observed SAMI now increase to 0.36 in JFM; however, it is still low in JAS. Further analyses reveal that warm months (from previous year October to March) generally have a higher reproducibility, correlation coefficients ranging from 0.25 to 0.43. The highest reproducibility occurs in December.

[14] The reproducibility of the interannual SAMI variability is dependent on the tropical Pacific forcing. The correlation coefficient between the SAMI and Nino3.4 index is −0.27 in JFM and −0.17 in JAS for observation, and December has the largest correlation of −0.34. The corresponding result for the simulation is −0.72 in JFM and −0.63 in JAS. It is the strong tropical forcing that determines the relatively better reproducibility of austral summer SAMI. The CAM2 model has a good performance in correctly generating the response to tropical Pacific forcing. This response is however overdone in intensity and even artificially significant in JAS. It seems that when considering the realistic variability and reproducibility, other factors should be taken into account; otherwise the SSTs signals would be over-estimated. Inspections on the regression pattern between SST anomalies and SAMI in December (Figure 4) reveal a dominance of negative anomalies over the middle and eastern equatorial Pacific in both the observation and the simulation. This further demonstrates the contribution of tropical Pacific in affecting the interannual variation of the SAM, with equatorial warm event corresponds to a negative phase SAM.

3. Summary and Discussion

[15] The SST-induced month-to-month and year-to-year SAM variations are examined by using the NCAR CAM2 model forced by observational SST covering the period 1950–2000, both in terms of ensemble-mean and single member simulations. Although the internal noise is larger than the external forced signal, still there is some corre-

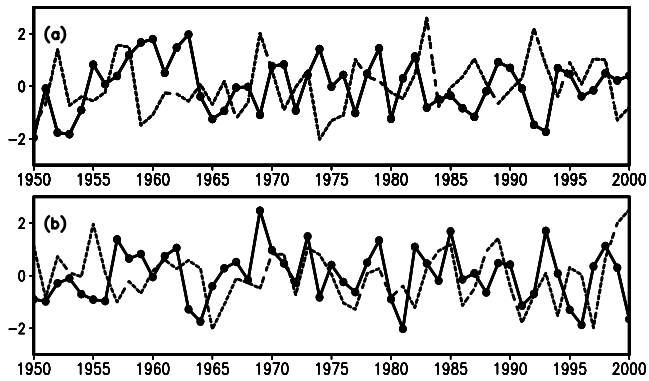

Figure 3. The (a) JFM and (b) JAS SAM index time series. The solid line with closed-circle corresponds to the observation, and the dashed line corresponds to the simulation.

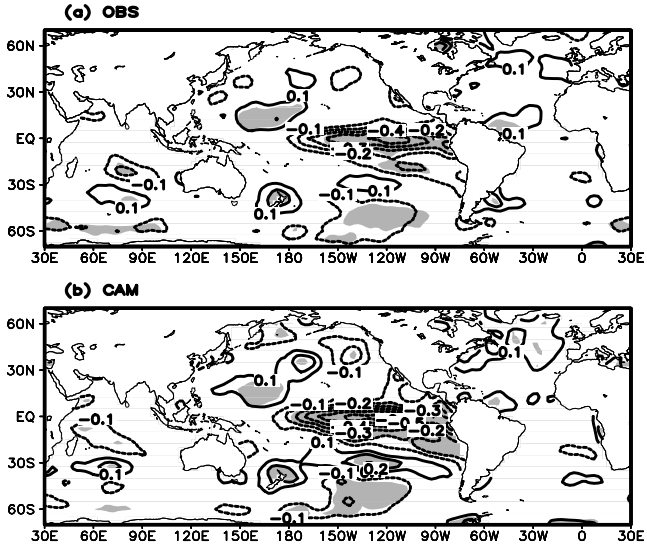

Figure 4. Regression of observational SST anomalies upon normalized SAMI in December for (a) observation and (b) simulation. Shaded regions are significant at 95% confidence level.

spondence between the AGCM and the observation in the temporal evolution of the SAM, indicating if global SSTs are known and prescribed to the AGCM, there would be some predictability to the SAM. The multi-members ensemble-mean is obviously superior to the single member simulation. The reproducibility of the SAM is greater during austral summer than winter, and the December SAMI has the highest reproducibility.

[16] The source of much of the predictability is tropical Pacific SST. Warm events over the middle and eastern equatorial Pacific correspond to a simultaneous negative phase austral summer SAM. *Silvestri and Vera* [2003] stated a significant correlation between the SAMI and ENSO index in austral spring, which is coherent with current study. Notice this is also the period when the SAM pattern amplifies upward into the stratosphere [*Thompson and Wallace*, 2000].

[17] Since the quality of the NCEP-NCAR reanalysis at the SH high-latitude is very poor before 1979 [*Renwick*, 2002], we re-compute the relevant results over the shorter period 1979–2000, and the conclusions remain unchanged.

[18] **Acknowledgments.** This work is jointly supported by the National Natural Science Foundation of China under Grant No. 40375029, 40233031 and the "Innovation Program of CAS" under Grant No. ZKCX2-SW-210 and KZCX3-SW-221. The authors thank NCAR Climate Variability Working Group for providing the model data and NCEP/NCAR for releasing the reanalysis data.

References

Carril, A. F., and A. Navarra (2001), The Interannual leading modes of the extratropical variability in the Southern Hemisphere simulated by the ECHAM-4 atmospheric model, *Clim. Dyn.*, *18*, 1–16.

Clare, G. R., B. B. Fitzharris, T. J. H. Chinn, and M. J. Salinger (2002), Interannual variation in end-of-summer snowlines of the Southern Alps of New Zealand, and relationships with Southern Hemisphere atmospheric circulation and sea surface temperature patterns, *Int. J. Climatol.*, *22*, 107–120.

Dawdy, D. R., and N. C. Matalas (1964), Statistical and probability analysis of hydrologic data, part III: Analysis of variance, covariance and time series, in *Handbook of Applied Hydrology: A Compendium of Water-Resources Technology*, edited by V. T. Chow, pp. 868–890, McGraw-Hill, New York.

Fyfe, J. C., G. J. Boer, and G. M. Flato (1999), The Arctic and Antarctic Oscillations and their projected changes under global warming, *Geophys. Res. Lett.*, *26*, 1601–1604.

Gong, D. Y., and W. S. Wang (1999), Definition of Antarctic Oscillation index, *Geophys. Res. Lett.*, *26*, 459–462.

Hall, A., and M. Visbeck (2002), Synchronous variability in the Southern Hemisphere atmosphere, sea ice, and ocean resulting from the annular mode, *J. Clim.*, *15*, 3043–3057.

Kalnay, E., et al. (1996), The NCEP/NCAR 40-year reanalysis project, *Bull. Am. Meteorol. Soc.*, *77*, 437–471.

Kidson, J. W. (1988), Interannual variations in the Southern Hemisphere circulation, *J. Clim.*, *1*, 1177–1198.

Kidson, J. W. (1999), Principal modes of Southern Hemisphere low-frequency variability obtained from NCEP-NCAR reanalyses, *J. Clim.*, *12*, 2808–2830.

Kidson, J. W., and I. G. Watterson (1999), The structure and predictability of the "High-Latitude Mode" in the CSIRO9 general circulation model, *J. Atmos. Sci.*, *56*, 3859–3873.

Kushner, P. J., I. M. Held, and T. L. Delworth (2001), Southern Hemisphere atmospheric circulation response to global warming, *J. Clim.*, *14*, 2238–2249.

Li, Z.-X. (1999), Ensemble atmospheric GCM simulation of climate interannual variability from 1979 to 1994, *J. Clim.*, *12*, 986–1001.

Limpasuvan, V., and D. L. Hartmann (2000), Wave-maintained annular modes of climate variability, *J. Clim.*, *13*, 4414–4429.

Marshall, G. (2003), Trends in the southern annular mode from observations and re-analyses, *J. Clim.*, *16*, 4134–4143.

Mo, K. C. (2000), Relationships between low-frequency variability in the Southern Hemisphere and sea surface temperature anomalies, *J. Clim.*, *13*, 3599–3610.

Nan, S., and J. Li (2003), The relationship between the summer precipitation in the Yangtze River valley and the boreal spring Southern Hemisphere annular mode, *Geophys. Res. Lett.*, *30*(24), 2266, doi:10.1029/2003GL018381.

Renwick, J. A. (2002), Southern Hemisphere circulation and relations with sea ice and sea surface temperature, *J. Clim.*, *15*, 3058–3068.

Sexton, D. M. H. (2001), The effect of stratospheric ozone depletion on the phase of the Antarctic Oscillation, *Geophys. Res. Lett.*, *28*, 3697–3700.

Shindell, D., R. Miller, G. Schmidt, and L. Pandolfo (1999), Simulation of recent northern winter climate trends by greenhouse-gas forcing, *Nature*, *25*, 452–455.

Silvestri, G. E., and C. S. Vera (2003), Antarctic Oscillation signal on precipitation anomalies over southeastern South America, *Geophys. Res. Lett.*, *30*(21), 2115, doi:10.1029/2003GL018277.

Stone, D. A., and A. J. Weaver (2001), Projection of climate change onto modes of atmospheric variability, *J. Clim.*, *14*, 3551–3565.

Thompson, D. W. J., and S. Solomon (2002), Interpretation of recent Southern Hemisphere climate change, *Science*, *296*, 895–899.

Thompson, D. W. J., and J. M. Wallace (2000), Annular modes in the extratropical circulation. Part I: Month-to-month variability, *J. Clim.*, *13*, 1000–1016.

Thompson, D. W. J., J. M. Wallace, and G. Hegerl (2000), Annular modes in the extratropical circulation. Part II: Trends, *J. Clim.*, *13*, 1018–1036.

Watterson, I. G. (2000), Southern midlatitude zonal wind vacillation and its interaction with the ocean in GCM simulations, *J. Clim.*, *13*, 562–578.

Watterson, I. G. (2001), Zonal wind vacillation and its interaction with the ocean: Implications for interannual variability and predictability, *J. Geophys. Res.*, *106*, 23,965–23,975.

Xue, F., H. Wang, and J. He (2003), Interannual variability of Mascarene high and Australian high and their influences on summer rainfall over East Asia, *Chin. Sci. Bull.*, *48*(5), 492–497.

T. Zhou and R. Yu, LASG, Institute of Atmospheric Physics, Chinese Academy of Sciences, Beijing 100029, China. (zhoutj@lasg.iap.ac.cn; yrc@lasg.iap.ac.cn)